frontiers | Frontiers in Materials

TYPE Original Research
PUBLISHED 28 April 2025
DOI 10.3389/fmats.2025.1414085

OPEN ACCESS

EDITED BY
Hamada Elsayed,
University of Padua, Italy

REVIEWED BY
Lipeng Xin,
Xi'an Jiaotong University, China
Chengying Bai,
Harbin Engineering University, China
Mona Sayed,
National Research Centre, Egypt

*CORRESPONDENCE
Yongzhen Wang,
wangyongzhen@tyut.edu.cn

RECEIVED 08 April 2024
ACCEPTED 27 March 2025
PUBLISHED 28 April 2025

CITATION
Zhou X, Wang Y, Lin R, Zhou R and Ma Y (2025) Adsorption of Ni^{2+}, Cu^{2+} and Co^{2+} ions on coal gangue-based porous ceramics. *Front. Mater.* 12:1414085. doi: 10.3389/fmats.2025.1414085

Adsorption of Ni^{2+}, Cu^{2+} and Co^{2+} ions on coal gangue-based porous ceramics

Xiaopeng Zhou[1,2], Yongzhen Wang[1,2]*, Renpeng Lin[1], Rui Zhou[2] and Yue Ma[1,2]

[1]College of Materials Science and Engineering, Taiyuan University of Technology, Taiyuan, Shanxi, China, [2]State Key Shanxi Joint Laboratory of Coal-based Solid Waste Resource Utilization and Green Development, Taiyuan University of Technology, Taiyuan, Shanxi, China

It is urgent to develop an adsorbent with low price and high removal rate of heavy metal cations for the treatment of wastewater. Herein, we report a novel coal gangue-based multiphase porous ceramic as an efficient and economic adsorbent for remove heavy metal cations. Due to the highly designed porous structure derived from the effect of pore-forming agents, the coal gangue-based multiphase porous ceramic adsorbent shows remarkable performance of the removal of Cu^{2+}, Co^{2+}, and Ni^{2+} from wastewater. Meanwhile, the microstructure and chemical composition of coal gangue-based porous ceramics have been characterized by X-Ray diffraction, Fourier transform infrared spectroscopy, and scanning electron microscope. Besides, the effects of the formula and particle size of silicon carbide on the structure of porous ceramics were also studied. Furthermore, the structure-function relationship between various reaction conditions and adsorption performance and the microstructure of adsorbent has been researched. In addition, the adsorption mechanism of complex porous ceramics on Cu^{2+}, Co^{2+}, and Ni^{2+} has been revealed by simulated calculation.

KEYWORDS

porous ceramics, mullite multiphase, adsorbent, adsorption mechanism, density functional simulation calculations (DFT)

1 Introduction

In recent years, the environmental pollution caused by the rapid development of industry cannot be ignored, among which heavy metals have extremely serious ecological risks due to their fluidity, toxicity, and wanton discharge (Qasem et al., 2021; Luo et al., 2024). Traditional removal methods include chemical precipitation, evaporation concentration, ion exchange, electrochemical treatment, adsorption, and membrane filtration (Kim et al., 2024). Among these methods, the adsorption method has great advantages over other methods in terms of treatment efficiency and cost, so the preparation of adsorbents with low price and high removal rate has become a research hotspot in the fields of environment and materials (Deng et al., 2017).

At present, low-cost adsorbents for the treatment of wastewater containing heavy metals mainly include ceramic (Chen et al., 2021), soil (Mazarji et al., 2023), biochar (Park et al., 2016), clay (Gu et al., 2019), and zeolite (Velarde et al., 2023). Among of the materials, porous ceramics have been considered as promising materials to purify heavy metal ions, because of its unique characteristics such as low density, high specific surface area and

good chemical stability (Chen et al., 2021). Ceramic based materials include mullite, alumina, silicon nitride, silicon carbide, diatomaceous earth, and iolite have thus been developed for solving the challenges in the treatment of heavy metal cations (Li et al., 2016; Han et al., 2017; Guo et al., 2016).

However, the performance of traditional porous ceramics is hard to meet the ever-growing needs of remove heavy metal cations. Coal gangue-based adsorbents, such as geopolymer and alkali activated material, have been employed as effective adsorbents for efficient removal of heavy metal cations, on account of the remarkable adsorption performance derived from its abundant 3D cross-linked structures (Mei et al., 2023; Li et al., 2022; Yan et al., 2018). Furthermore, the advantages of the abundant reserves, low economic cost and simple production methods make coal gangue-based adsorbents become sustainable and low-cost. Therefore, mullite complex porous ceramics based on coal gangue are promisingly economical absorbers with outstanding ability of eliminating heavy metal cations (Sun et al., 2022; Zhang et al., 2020). In addition, density functional theory (DFT) computational simulations including dynamic, thermodynamic and functional theory are novel methods to make in-depth research about the adsorption property and characteristics of materials (Ren et al., 2022; Xu et al., 2021).

Herein, we construct a novel coal gangue-based multiphase porous ceramic via simple sintering foaming method as a high effective and economic adsorbent for well treatment of heavy metal cations. Due to the unique porous structure derived from the effect of pore-forming agents, the coal gangue-based multiphase porous ceramic adsorbent exhibit remarkable performance of the removal of Cu^{2+}, Co^{2+}, and Ni^{2+} from wastewater. The microstructure and chemical composition of coal gangue-based porous ceramics have been characterized by X-Ray diffraction (XRD), Fourier transform infrared spectroscopy (FTIR), and scanning electron microscope (SEM), and the effects of the formula and particle size of silicon carbide on the structure of porous ceramics were also studied. Furthermore, the structure-function relationship between the content of additives, adsorption time/temperature and adsorption performance and the microstructure of adsorbent has been explored. In addition, the adsorption mechanism of complex porous ceramics on Cu^{2+}, Co^{2+}, and Ni^{2+} has been revealed by simulated calculation. Consequently, the coal gangue-based multiphase porous ceramic adsorbent may shed fresh light on purification of wastewater.

2 Experimental parts

2.1 Raw materials and equipment

Coal Gangue (origin: Yangquan, Shanxi), silicon carbide, sodium carbonate, alumina, sodium carboxymethyl cellulose (CMC). The raw material is coal gangue, which consists mainly of silicon dioxide and alumina. The chemical composition of coal gangue is detected by mass spectrometry and the results are shown in Supplementary Table S1. Sodium carbonate, silicon carbide, alumina, carboxymethyl cellulose (CMC), China National Pharmaceutical Group Chemical Reagent Co. Ltd. The water used in the laboratory is self-made distilled water. The main chemical composition and phase composition of coal gangue material are shown in Supplementary Table S1 and Supplementary Figure S1 by X-ray diffraction. It can be seen from the table that the main components of coal gangue are SiO_2, Al_2O_3, containing a small amount of sulfur and iron. According to the semi-quantitative analysis of XRD data by using the theory of RIR value of Jade 6, it is found that the main phases are quartz, aged stone, some pyrite and a little dolomite. The composition data are consistent, and the diagram shows that the content of silicon dioxide in coal gangue is on the high side. It is a problem to be considered in the follow-up experiment. In addition, instruments such as Beaker, centrifuge tube, mortar, corundum boat and crucible are needed in the experiment (Supplementary Table S2).

2.2 Principle of preparation

As shown in Figure 1, when the temperature is higher than 900°C, the silicon carbide powder reacts with oxygen and other oxides in the furnace to produce CO and CO_2 (Roy et al., 2014). Compared with $CaCO_3$, $CaSO_4$, and dolomite, silicon carbide can increase the porosity of ceramics more efficiently (Xia et al., 2022), and obtain more widely distributed pores. Because of its excellent properties, it plays an indispensable role in asymmetric ceramic adsorption materials. The coal gangue itself contains a small amount of metal elements, which is conducive to promoting the formation of mullite reaction between alumina and silica, this makes silicon carbide easier to break down and produce more gas to keep the pore size under control (Li et al., 2022). The mullite is formed at temperatures above 1,400°C (Aksay and Pask, 1974), and that the temperature required for the preparation of mullite is reduced by the presence of a certain amount of impurities in the material under test. The phase diagram shows in Figure 2 that the best condition for forming mullite is between 20% and 30% of SiO_2. Therefore, it is necessary to add some alumina in the following experiments, as far as possible, the silicon dioxide impurities in the ceramic can be effectively reduced to ensure that the porous ceramic is a mullite-silicon carbide composite phase.

2.3 Preparation of porous ceramics

The raw materials were prepared by ball milling of 15% silicon carbide, a certain amount of alumina and sodium carbonate, and 1.5% sodium carboxymethyl cellulose (CMC). After 0.6 g of the mixed material was used to press 10 MPa at pressure for 4 min, the ceramic samples were obtained. And the samples were heated to 1,200°C–1,325°C at the rate of 5°C/min in muffle furnace, and then cooled to normal temperature after holding for 90 min.

2.4 Adsorption experiment

In order to investigate the effects of porous ceramic materials on Cu^{2+}, Co^{2+}, and Ni^{2+}, the particle size, adsorption time, and their effects on the preparation of porous ceramics were studied. The effects of adsorption temperature, adsorption time, and initial solution concentration on adsorption performance were also

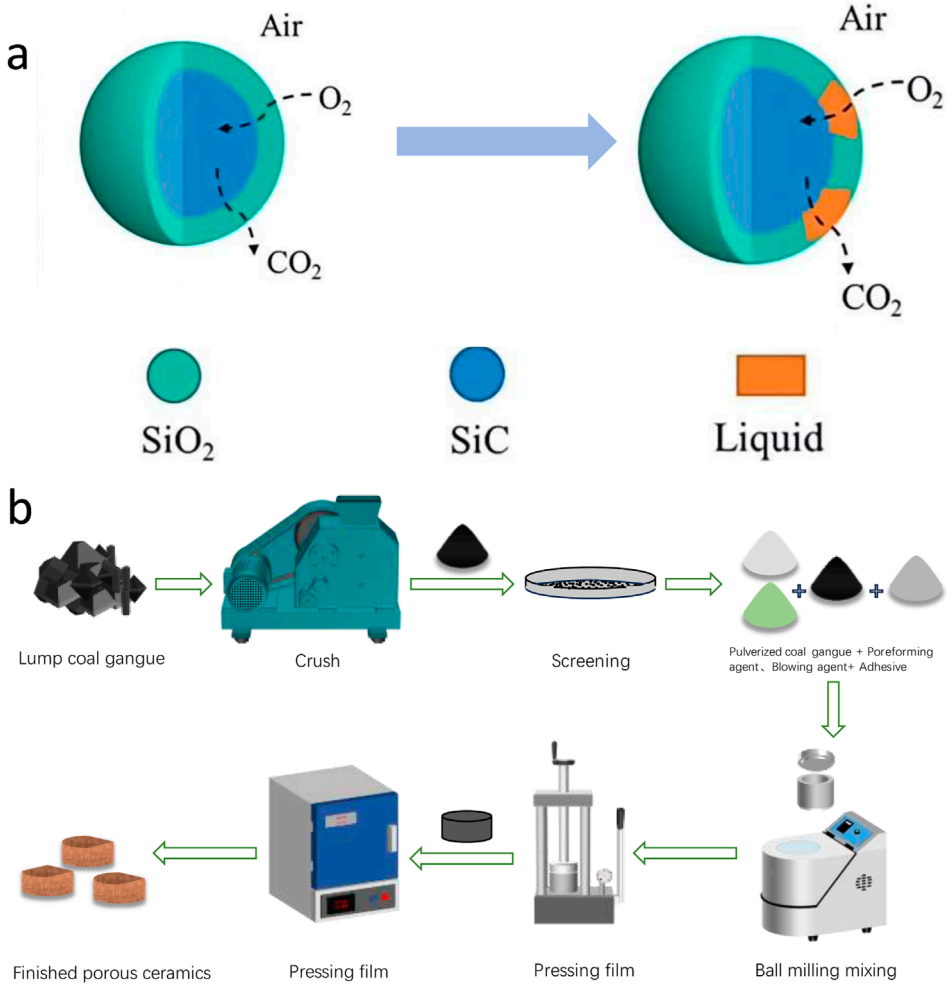

FIGURE 1
(a) Decomposition mechanism diagram of SiC pore preparation; **(b)** Process of preparing porous ceramics from coal gangue.

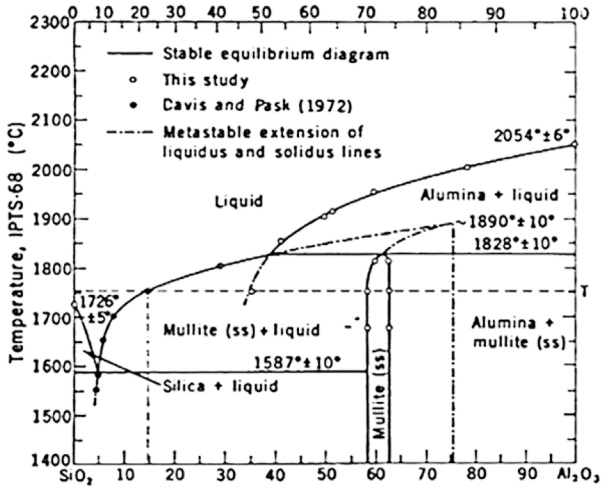

FIGURE 2
Mullite binary phase diagram (Aksay and Pask, 1974).

investigated. Cu^{2+}, Co^{2+}, and Ni^{2+}were prepared using chemically pure reagents Cu^{2+}, Co^{2+}, and Ni^{2+}. At the end of the reaction, extract the treated liquid with a dropper, measure and analyze the content of Cu^{2+}, Co^{2+}, and Ni^{2+}in the solution, and calculate the adsorption capacity. Each sample was set with some parallel samples and the experimental data was averaged.

3 Results and discussion

3.1 Effect of reaction conditions on porous ceramics

Considering the influence of temperature, sodium carbonate content and alumina content on the preparation of porous ceramics, it is necessary to prepare the porous ceramics at different reaction conditions. Therefore, the optimum reaction conditions can be obtained by rational regulate the conditions.

Figure 3a shows the XRD data of mullite and silicon carbide for the multi-phase porous ceramics with calcination temperature

10.3389/fmats.2025.1414085

ranged from 1,250°C to 1,325°C. Try to lower the temperature while holding the original phase. It is found that when the temperature is below 1,250°C, the peak degree of silicon carbide increases, even quartz phase appears. Therefore, the suitable calcination temperature is 1,250°C to ensure stable phase formation of porous ceramics. Besides, it can be seen from Figure 3b and Supplementary Table S3 that the addition of sodium carbonate at 1.5%, from the XRD can be seen in its composition of quartz content is too high. The results show that the reaction is not complete, mullite phase is not complete reaction, there are higher impurities. When the content of sodium carbonate is 6%, there are more impurities in quartz phase and no holes in the ceramics. Not suitable as a porous ceramic material. The composition of the ceramic films with 3%, 4%, and 5% silicon carbide can be observed by XRD. There is obvious mullite + silicon carbide phase. Besides, the ability of prevent crushing stress increased by sodium carbonate content. When the amount of sodium carbonate is 5%, the water absorption effect and the mechanical strength is the best, which is better than previous work (Mei et al., 2023; Li et al., 2022; Yan et al., 2018). Therefore, the best addition of sodium carbonate is 5% for optimal boost the porosity of materials. In addition, Figure 3c shows the effect of alumina content. The peak of silicon carbide was the highest when the addition of alumina was 1.5% and 3%. It shows that the reaction efficiency of silicon carbide is too low in the sintering process, so it is necessary to increase the amount of alumina to ensure the reaction. When the addition of alumina reaches 7%, the peak of alumina appeared, and the silicon dioxide was still high. The results show that the composition of Mullite is about 60% and that of silicon carbide is about 32% by Quantitative analysis the XRD data by Jade 6. So that the impurities are less than 8%, thus the mullite and silicon carbide multiphase porous ceramic materials are obtained.

Furthermore, the effect of SiC particle size has been detected by SEM and XRD. The pore size of porous ceramic prepared by silicon carbide with pore size of 300 mesh (48 μm) is the most uniform distribution which is compared to silicon carbide with pore size of 200 mesh and 500 mesh (Figures 4a–d; Supplementary Figure S1). And there is no quartz at the characteristic peak of 2θ = 46° when the size of silicon carbide particle is added at 300 mesh, which proves that the content of quartz is low. The more obvious silicon carbide and mullite peak, indicating that the formation of ceramic mullite phase (Figure 4e). Therefore, 300 mesh silicon carbide can be used as a pore-forming agent. It can be seen that it contains silicon and oxygen in the display composition of EDS (Supplementary Figures S1A–F). The content of oxygen is high, it contains quartz components.

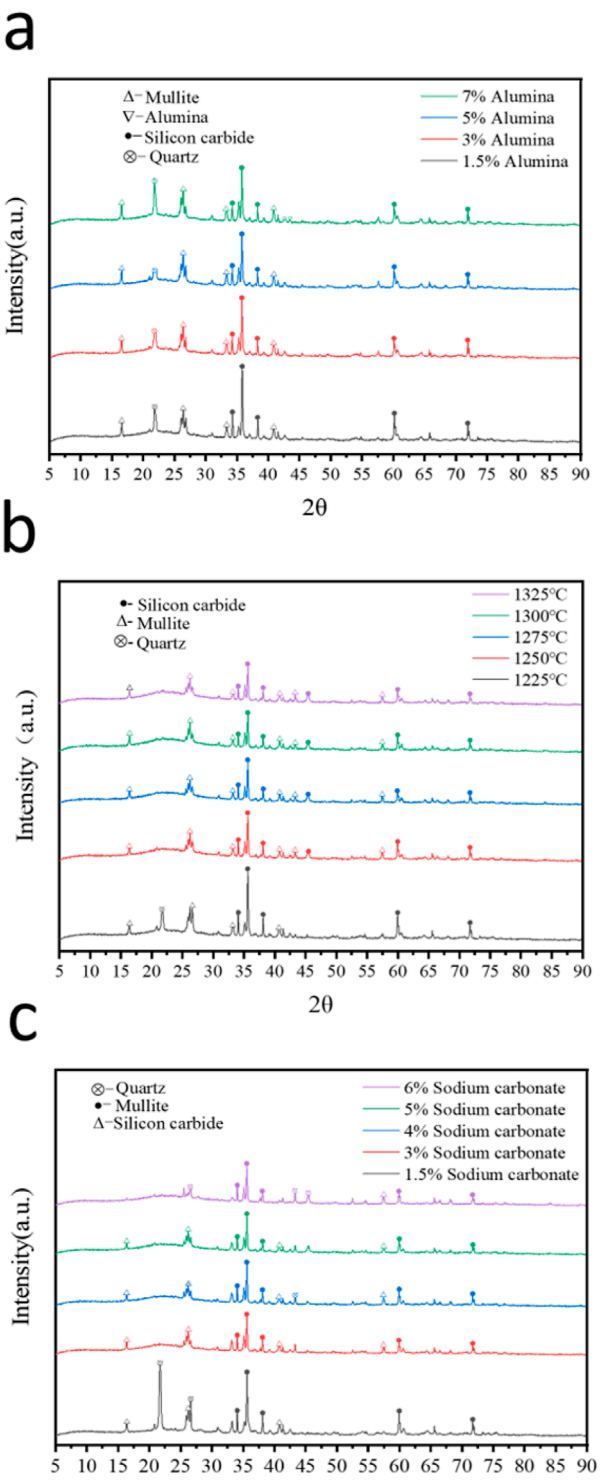

FIGURE 3
XRD patterns of porous ceramics **(a)** at different calcination temperatures, **(b)** with different sodium carbonate content and **(c)** alumina content.

3.2 The influence of different factors on adsorption performance

The effect of initial concentration of solution on the adsorption properties are shown in Figure 5 and Figure 6. It can be seen that in the concentration range of 40–175 mg/L, as the initial concentration of the solution increases, the adsorption capacity of coal gangue based porous ceramic materials for Cu^{2+}, Co^{2+}, and Ni^{2+} continues to increase. When the adsorption capacity reaches a certain amount, it tends to flatten out, and then the concentration gradually increases. When the amount reaches a certain value, it remains unchanged; The solution concentration is the same, except for coal gangue porous ceramic materials. It can be seen from the adsorption effect of porous ceramic materials on three types of metal cations. The adsorption effect of porous ceramic materials is Ni^{2+} > Cu^{2+} > Co^{2+}. Moreover, porous ceramic materials have a higher

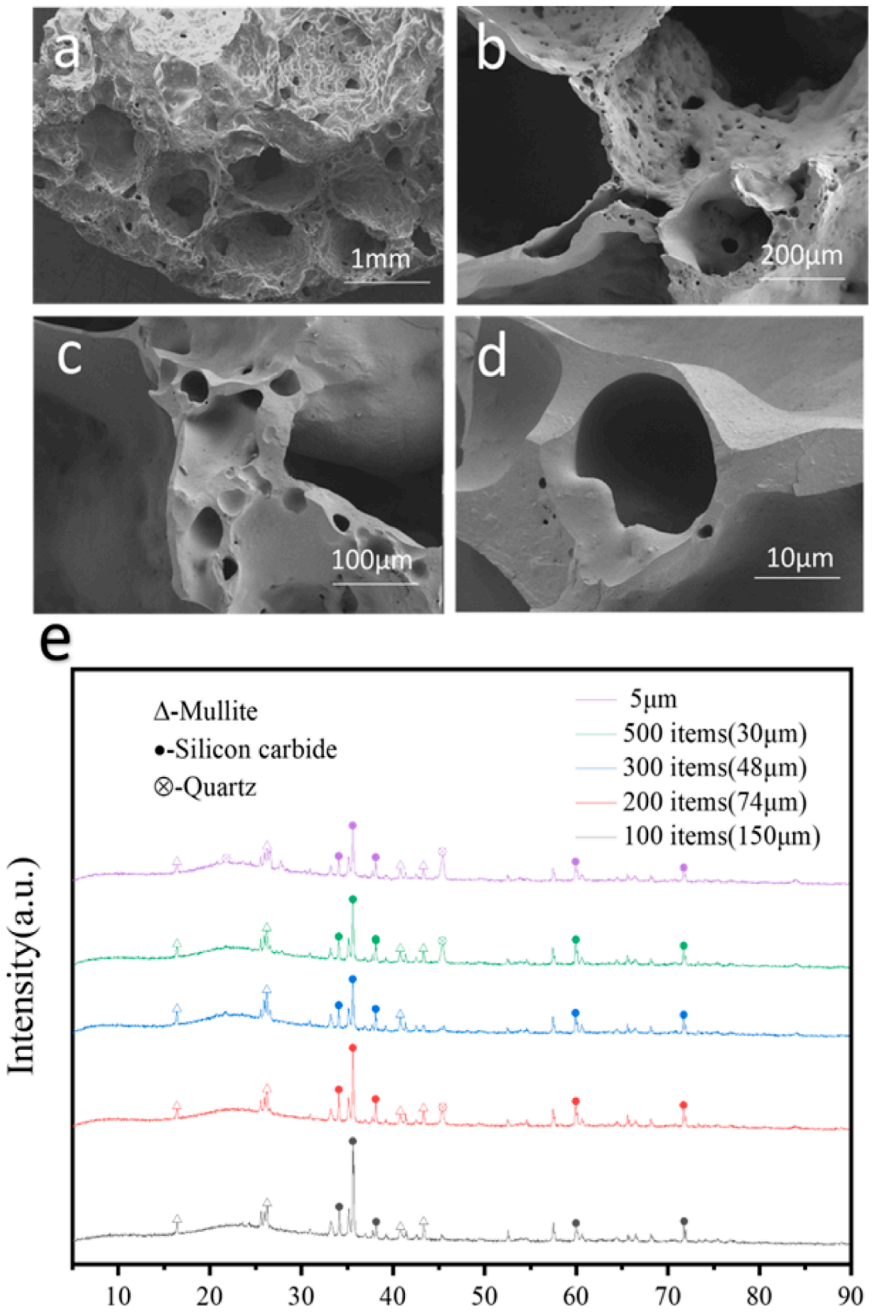

FIGURE 4
(a–d) SEM images of the porous ceramic prepared by silicon carbide with pore size of 300 mesh (48 μm); **(e)** XRD patterns of porous ceramics with different SiC particle sizes.

adsorption capacity for Ni^{2+} (Supplementary Table S4). At the same time, it can also be understood that when the concentration of the ionic solution reaches 100 mg/L, the solution concentration should be further increased. There is no significant change in the adsorption effect. Therefore, the appropriate value for the adsorption of these three metal ions by porous ceramic materials is 100 mg/L.

In addition, the influence of adsorption time/temperature on adsorption performance are also be explored in Figure 7. When the concentration of the three components is 100 mg/L respectively, the adsorption PH is 7, the oscillation time is 720 min, and the oscillation rate is 180 r/min, the addition amount of porous ceramic material is 10 g/L. The influence of modification or not on the adsorption capacity of the three components is shown in the figure below. From the experimental results, the initial reaction rate is very fast, at this time the reaction mainly occurred in the surface of coal gangue-based porous ceramics, some of the existence of physical adsorption. With the passage of time, part of Cu^{2+}, Co^{+}, Ni^{2+} were added into the porous ceramic materials, and gradually occupied the positions. With the passage of time, more and more adsorption sites were found due to the large amount of

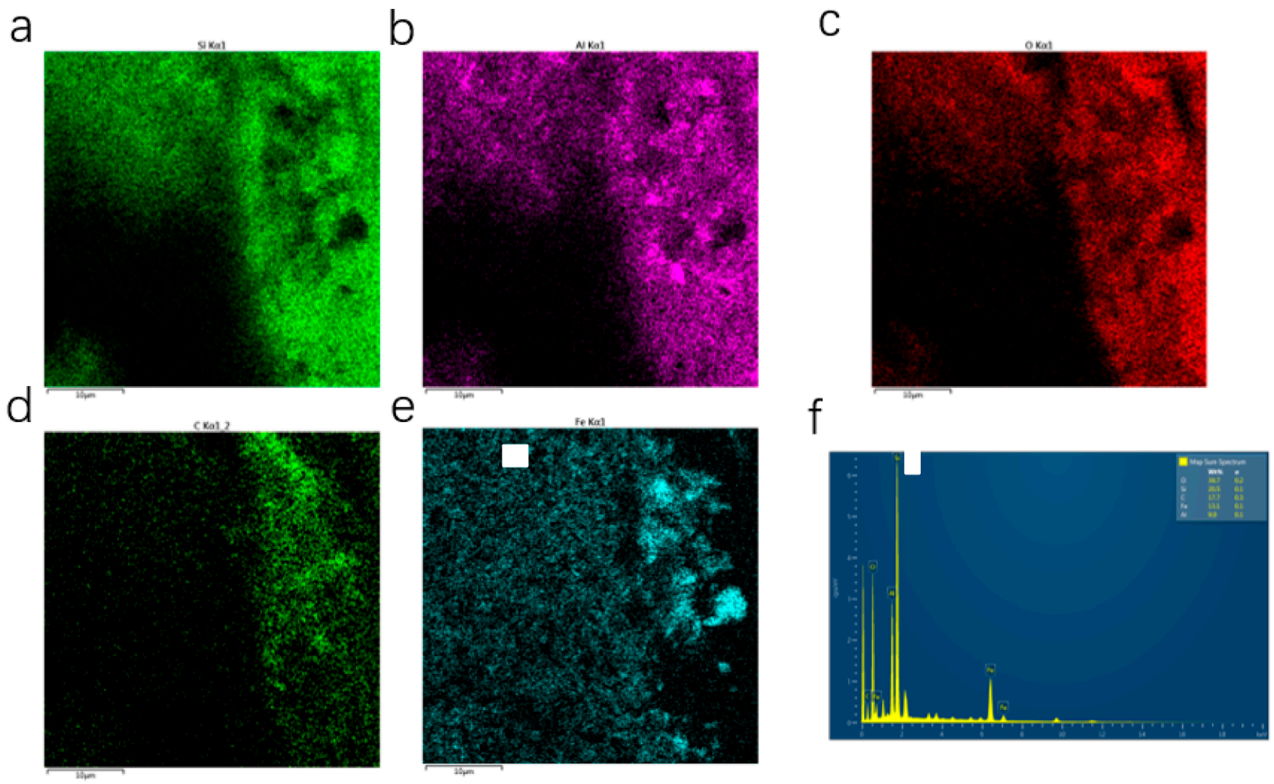

FIGURE 5
(a–e) EDS images of the porous ceramic prepared by silicon carbide with pore size of 300 mesh (48 μm); **(f)** Ceramics are analyzed for component content in EDS.

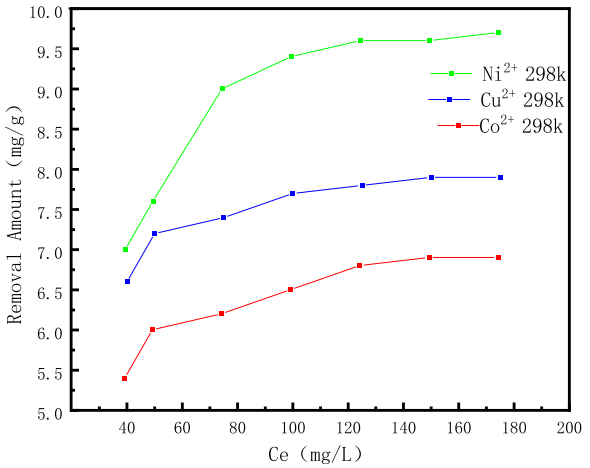

FIGURE 6
The effect of initial concentration of solution on the adsorption properties of Cu^{2+}, Co^{2+} and Ni^{2+} ions.

adsorption (Figures 7a–c). There are fewer and fewer sites available for efficient adsorption, which slows down the adsorption to a state of adsorption equilibrium. At this time, the adsorption rate inside and outside of coal gangue-based porous ceramic material decreases to reach saturation, so that the amount of adsorption does not change.

From the graph, it can be seen that the initial concentration of the solution varies within the range of 40–175 mg/L. Under three different temperature conditions of 20°C, 30°C, and 40°C, the adsorption capacity of coal gangue based porous ceramic materials for Cu^{2+}, Co^{2+}, and Ni^{2+} has been improved, respectively (Supplementary Table S5). The analysis result shows that under the same initial concentration the temperature increases with the adsorption capacity increases due to the more thorough diffusion of ions on the surface, allowing more ions to enter the surface and interior of porous ceramics (Figures 7d–f). And the increase in temperature is conducive to the increase of active sites on the surface. To be specific the adsorbent properties of novel coal gangue-based multiphase porous ceramic is close to or better than the recently reported strategies for purification of wastewater (Mei et al., 2023; Li et al., 2022; Yan et al., 2018).

3.3 Characterization of porous ceramics

Impeccable characterizations are necessary to understand the pore structure and chemical compositions of the material. Figure 6 shows the nitrogen adsorption desorption curve and pore size distribution curve of the coal gangue based multi-porous ceramic material sample. According to the division of adsorption isotherms by IUPAC, the sample belongs to Type IV adsorption isotherm, and there is an inflection point at $P/P_0 = 0.1$ in the lower pressure section, and the adsorption capacity in the lower pressure section

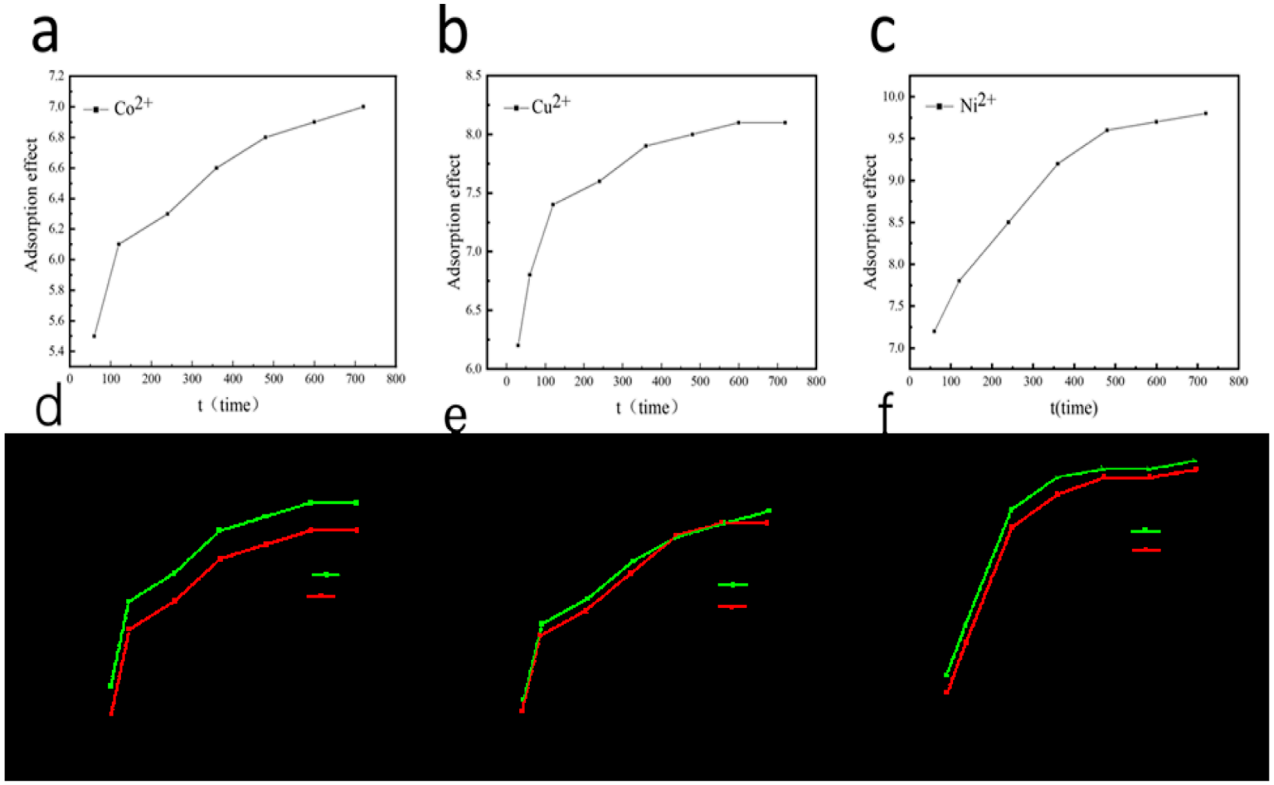

FIGURE 7
(a–c) The influence of adsorption time and **(d–f)** adsorption temperature on adsorption performance for Ni^{2+}, Cu^{2+}, Co^{2+}.

rises gently. It shows that the interaction between the surface of the sample and nitrogen molecules is weak, and the micropore content of the sample is low. With the increase of relative pressure, the capillary condensation of nitrogen occurs in the mesoporous pore channel. When the pressure decreases, the condensed liquid nitrogen volatilization leads to the difference between the desorption curve and the adsorption curve to form a hysteresis ring. Compared with the standard hysteresis ring type, the curve is H4 hysteresis ring indicating that the sample pore structure is irregular and mainly consists of narrow pores with the accumulation of sheet particles.

The adsorption curve is located at P/P_0 = 0.99, the maximum nitrogen adsorption capacity of the sample is 26.7513 mL, and the volume of 1 mL nitrogen after condensation under standard condition (STP) is 0.001547 mL, so the total pore volume of the sample is equal to 0.0418 cm^3/g. For the range of P/P_0 = 0.1–0.29 in the lower pressure section, the specific surface area calculated by bet method is 17.6125 m^2/g. It can be seen from the pore size distribution curve that the pore size of the sample is mainly distributed in the range of 2–50 nm, and the maximum pore size is concentrated in 3.59 nm, showing typical characteristics of mesoporous materials (Figures 8a,b).

Figures 8c,d shows the absorption peak at 3,589 cm^{-1} is the stretching vibration of O-H (Musso et al., 2014), the absorption peak at 3,443 cm^{-1} is the stretching vibration of OH (Musso et al., 2014), the absorption peak at 1,780 cm^{-1} is the stretching vibration of C=O, and the absorption peak at 1,623 cm^{-1} (Martra et al., 1999) is the variable Angle vibration of -OH. The absorption peak at 1,100–1,000 cm^{-1} is the antisymmetric stretching vibration of Si-O-Si (Eren and Afsin, 2008; Fonseca et al., 2009), the absorption peak at 1,000–900 cm^{-1} is the stretching and bending vibration of Al-OH, the absorption peak at 785 cm^{-1} is the symmetric stretching vibration of Si-O-Si, and the absorption peak at 729 cm^{-1} is the vertical vibration of Al-OH. Among them, according to the PDF figure, the absorption peak at 500–550 cm^{-1} (Musso et al., 2014; Eren and Afsin, 2008; Dawodu and Akpomie, 2014) is the stretching vibration of Al-O-Si. It can be seen that the surface has chemical bonds such as ≡ Si-O, ≡ Al-O, ≡ Al-OH, and the potential of the suspension system is negative, which is the structural basis of its excellent adsorption performance. From the adsorbed material, the characteristic peaks of 3,589 and 3,443 cm^{-1} are wide and disappear obviously (Tan et al., 2023), which indicates that Ni^{2+}, Co^{2+}, and Ni^{2+} in wastewater combine with oxygen atoms and carbonyl groups on the surface of coal gangue based porous ceramics, and chemical reactions occur.

BET characterization can be seen that there are many through holes at this time, and most of them are mesopores and macropores. FT-IR showed that the adsorption of three heavy metal ions by porous ceramic materials was mainly based on the combination of hydroxyl groups and metal ions. On the whole, when the ceramic material is just in contact with the solution, the hydroxyl group on its surface is mainly combined with metal ions to form effective chemical bonds to form adsorption effects.

It can be seen from the Figures 9a–c, the size of the electron microscope is 1 micron, it can be seen that the porous ceramic

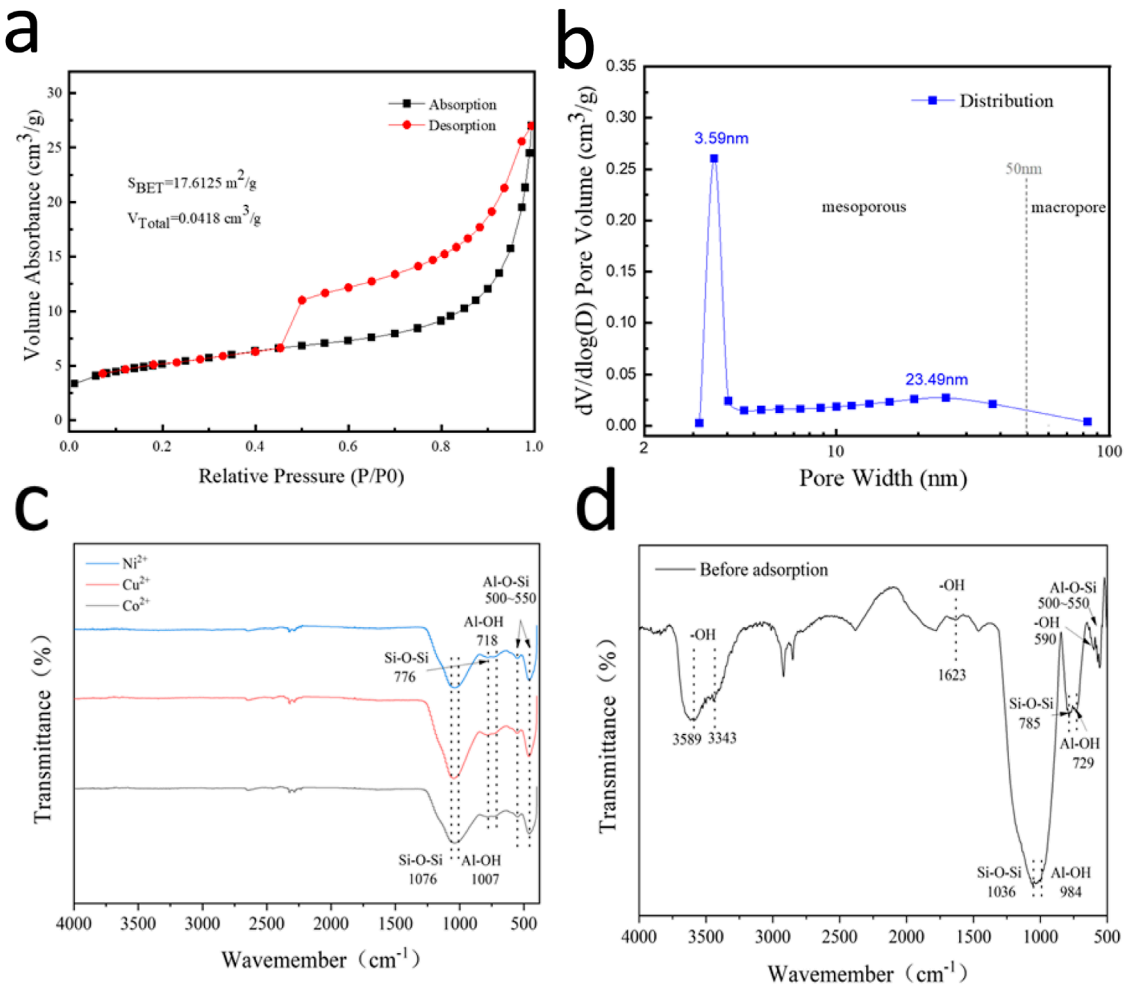

FIGURE 8
(a) Nitrogen adsorption-desorption curve **(b)** plot of pore size distribution; **(c)** FTIR spectra of porous ceramics after adsorbing Ni^{2+}, Cu^{2+}, Co^{2+} and **(d)** initial porous ceramics.

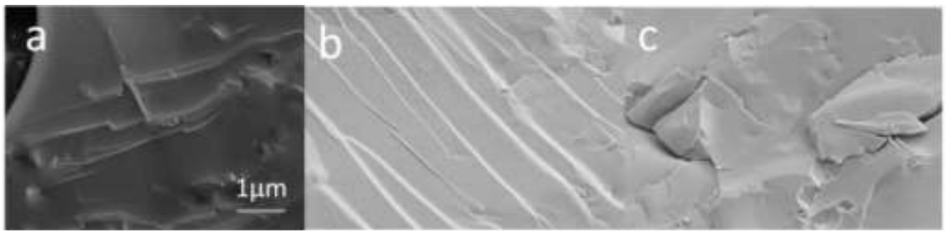

FIGURE 9
(a–c) SEM image of porous ceramic surface (1 μm).

surface has fish scale pattern and step type surface. It shows that the crystalline phase of mullite is formed during the growth of ceramics. According to SEM, it can be seen from (b) that the surface of porous ceramics has a fish-scale pattern and a ladder-type surface (Jiao et al., 2023; Wei et al., 2020). It can be seen that it forms a crystalline phase, which provides a basis for computer simulation of the configuration of the adsorbed substrate.

3.4 Adsorption effect of porous ceramics

3.4.1 Adsorption kinetics simulation

The quasi-first-order kinetics and quasi-second-order kinetics models are classical models for studying adsorption kinetics. The theoretical basis of the models is kinetics, which reflects the changes of adsorption rate under the influence of PH value of solution,

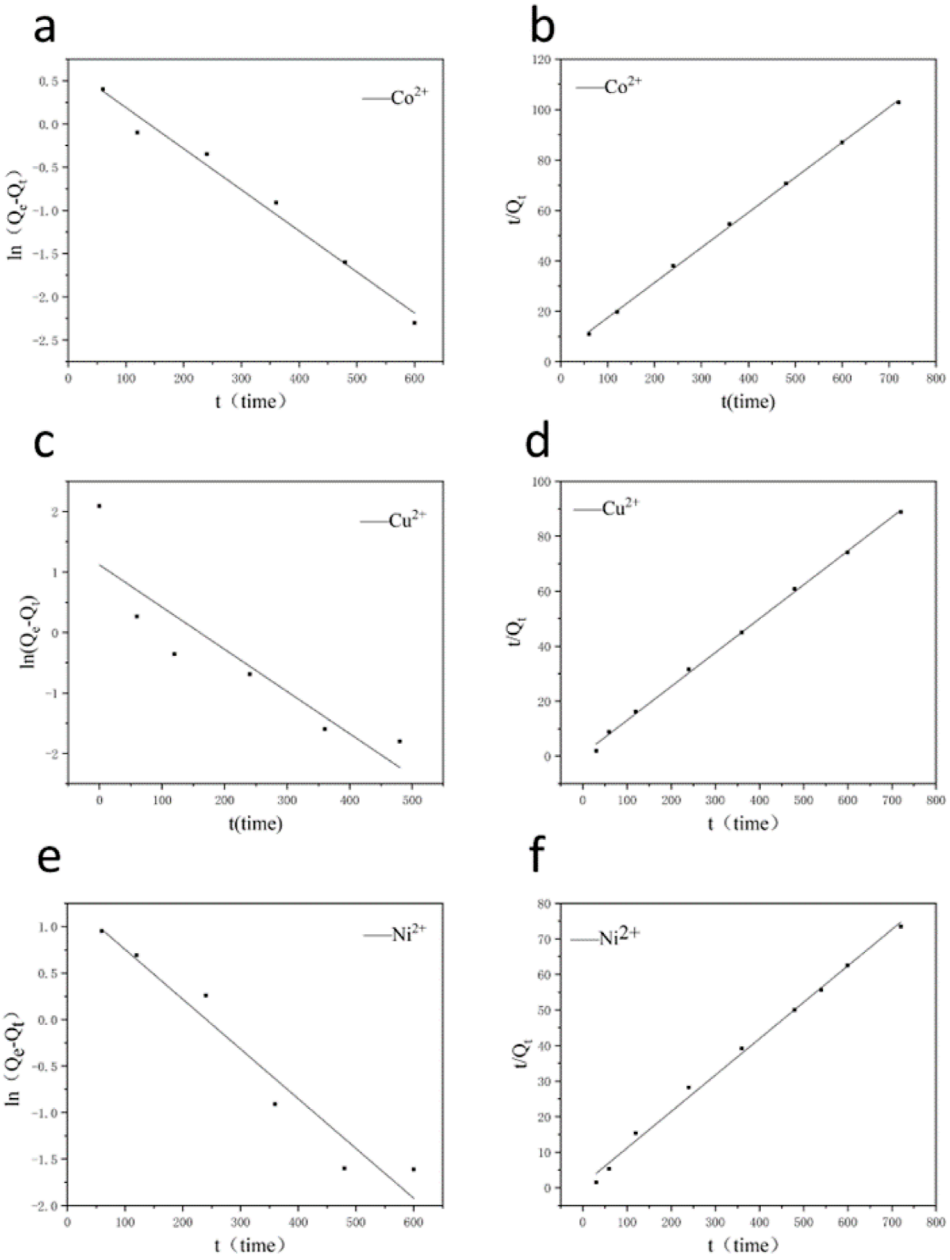

FIGURE 10
(a,c,e) The fit line of the Quasi-first-order dynamics and **(b,d,f)** Quasi-second-order dynamics.

adsorption input, modification conditions, initial concentration of solution, etc. It can be used to judge the direction of material transfer in the adsorption process and predict the reaction rate. Both models can predict the maximum adsorption amount of adsorbent in theoretical adsorption equilibrium (Equations 1, 2).

The quasi-first-order kinetic equation:

$$\ln(q_e - q_t) = \ln q_e - k_1 t \quad (1)$$

The quasi-second-order kinetic equation:

$$\frac{t}{q_t} = \frac{1}{k_2 \times q_e^2} + \frac{t}{q_e} \quad (2)$$

Where q_e–the adsorption amount of metal ions at theoretical adsorption equilibrium (mg/g), the adsorption amount of heavy metal ions at q_t–t (mg/g), and the adsorption amount of heavy metal ions at q–the adsorption amount of heavy metal ions at adsorption equilibrium (mg/g); k_1–The first-order kinetic adsorption constant (min^{-1}) can be calculated from the slope of ln (q_e-q_t) and t, and k_2–the second-order kinetic adsorption rate constant [mg/(g·min)] can be calculated from the intercept of Equation 2.

The adsorption capacity of multi-porous ceramics in coal gangue was measured over time. The adsorption kinetics were shown in Figures 10a,b, and the dynamic parameters were shown in Supplementary Table S6. According to the analysis of adsorption

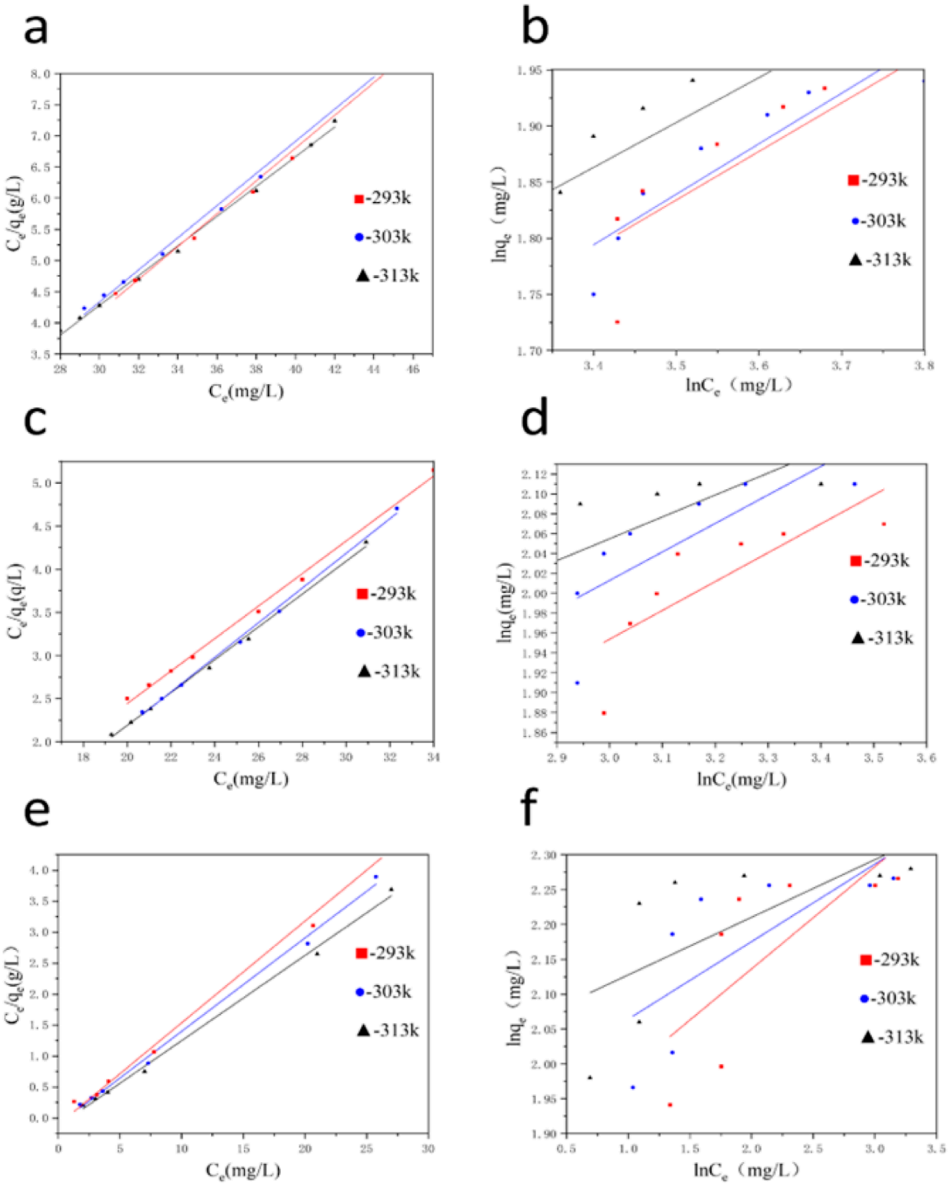

FIGURE 11
(a–f) Adsorption curve temperature of Co^{2+}, Cu^{2+}, Ni^{2+}.

capacity and fitting kinetic parameters, it was found that the equilibrium adsorption capacities of Cu^{2+}, Ni^{2+}, and Co^{2+} in the three ion samples with the initial concentration of 100 mg/L were 8.13, 9.66, and 6.99 mg/g, which were in good agreement with the experimental values. The quasi-second-order kinetic model is more suitable to explain the kinetic behavior of porous ceramics, which shows that the adsorption of Cu^{2+}, Ni^{2+}, and Co^{2+} of multi-phase porous ceramics prepared from coal gangue is mainly chemical adsorption (Figures 10c–f).

3.4.2 Thermodynamic simulation of adsorption

In order to better understand the adsorption process of coal gangue based multi-porous ceramic materials, Langmuir model and Freundlich model were adopted in this experiment to fit the adsorption of Cu^{2+}, Co^{2+}, and Ni^{2+} on porous ceramic materials, so as to explore the adsorption mechanism.

The experiments of Langmuir and Freundlich isothermal model fitting were analyzed according to Figure 11 and Supplementary Tables S7–S9. It can be seen that in the fitting of Langmuir simulation, the correlation coefficient (R^2) is in the range of 0.9929~0.9972, which proves that the adsorption of Cu^{2+}, Co^{2+}, and Ni^{2+} is in good agreement with the modified isotherm (Supplementary Tables S7–S9). In the fitting of Freundlich model, The R^2 value of Langmuir model was higher than that of Freundlich model in the range of 0.6060 to 0.8313. In previous studies, Langmuir model was often used to fit the adsorption of heavy metal ions on adsorbents (Yao et al., 2019), biomass (Zhu et al., 2016), and graphene-based materials (Sui et al., 2020). Therefore,

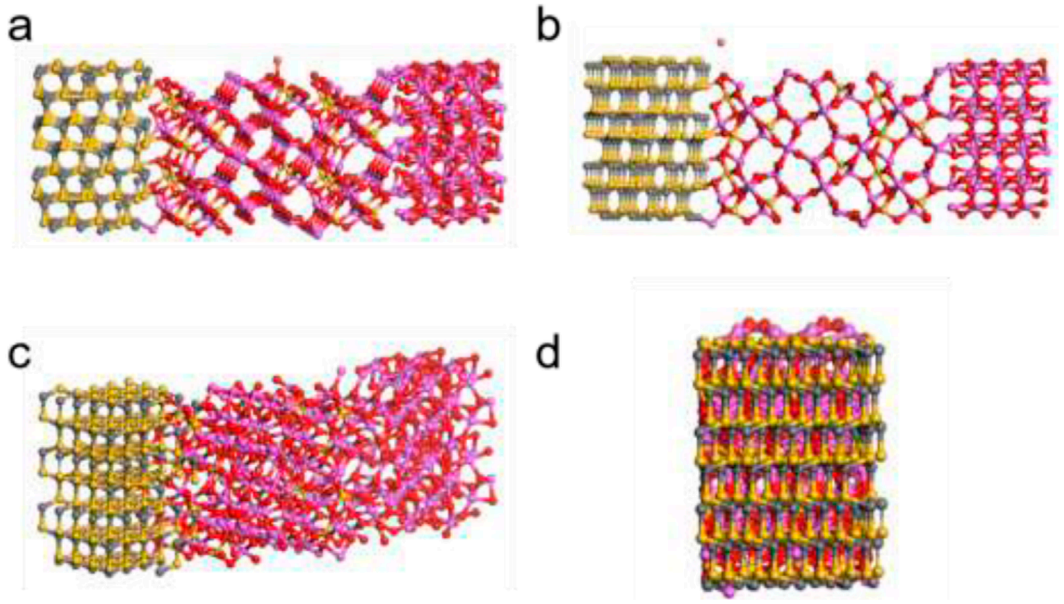

FIGURE 12
(a) Silicon carbide angle viewing; **(b)** Mullite viewing angle; **(c)** Front and **(d)** side view.

according to the fitting results of Langmuir model, the adsorption process of coal gangue based porous ceramic adsorption material was discussed. The adsorption process of Cu^{2+}, Co^{2+}, and Ni^{2+} on porous ceramic materials is single-layer uniform adsorption, and chemical adsorption is the main process (Guo et al., 2023). Compared with Langmuir models of different temperatures, the higher the temperature, the stronger the adsorption capacity of the material, that is, temperature rise is conducive to adsorption. In addition, at the conventional operating temperature (293 K), the K_L value is between 0 and 1.0 L/g, indicating that the adsorption effect is good. In summary, at the same temperature and different initial concentration, the adsorption process is mainly homogeneous monolayer adsorption, and the temperature increases to promote the reaction.

3.5 Simulated calculation of porous ceramics performance

We simulated the adsorption of porous ceramic components with three kinds of ions under the condition of water absorption, and the process and results are as follows:

We used the DFT as implemented in the MS in all calculations. The exchange-correlation potential is described by using the generalized gradient approximation of Perdew-Burke-Ernzerhof (GGA-PBE). The projector augmented-wave (PAW) method is employed to treat interactions between ion cores and valence electrons. The plane-wave cutoff energy was fixed to 500 eV. Given structural models were relaxed until the Hellmann–Feynman forces smaller than −0.02 eV/Å and the change in energy smaller than 10^{-5} eV was attained. The vacuum thickness was set to be 25 Å to minimize interlayer interactions. During the relaxation, the Brillouin zone was represented by a Γ centered k-point grid of 6 × 6 × 1. Grimme's DFT-D3 methodology was used to describe the dispersion interactions among all the atoms in adsorption models.

The adsorption energy (E_{ads}) of a complex formed between two molecules, A and B, can be calculated using the following equation:

$$E_{ads} = E_{complex} - (E_A + E_B)E_{ads}$$

where:

$E_{complex}$ is the total energy of the molecular complex of A and B.

E_A and E_B are the total energies of isolated molecules A and B, respectively.

From the adsorption simulation (Supplementary Tables S10–S12), it can be seen that for the two main types of oxygen and aluminum in contact with the surface of porous ceramic materials, overall, the elements of metal ions tend to form valence bonds with the oxygen element on the surface of the ceramic material, which is more stable and conducive to adsorption. And the results indicate that the adsorbed ones tend to bond with oxygen or hydroxyl groups on the atomic surface rather than with aluminum in terms of reaction.

Moreover, the adsorption energy of porous ceramic materials for Ni^{2+} is greater than that of Cu^{2+} and Co^{2+} in all chemical energies during valence bonding. In chemical adsorption, although the chemical energies of Co^{2+} and Cu^{2+} ions in contact with different elements on the surface of porous ceramic materials vary, the overall adsorption is mainly based on the contact between oxygen elements and metal ions. Therefore, the adsorption capacity of Cu^{2+} is greater than that of Co^{2+}.

In terms of physical adsorption, compared to chemical adsorption. Its adsorption energy is smaller, mainly due to van der Waals forces. Due to the minimum ionic radius of Ni^{2+} being 69 p.m., it is easier to come into contact with the surface of porous ceramics. Therefore, it has the highest adsorption energy and the best adsorption effect. For Cu^{2+}, a bond length of 2.176 Å is a

hexahedral octahedron with two long bonds and four short bonds. This makes it relatively easy to form chemical bonds, but less prone to physical adsorption (Figure 12).

From the simulated structure, it can be seen that Al-O-Al has a larger main bond angle and bond length, with a coordination bond number of 3 (Supplementary Table S13), resulting in a looser surface and larger pores. Compared with silicon carbide, it has better adsorption capacity. This allows for more contact between metal ions under appropriate conditions. Due to the coordination number of Si-O being 4, the pores are uneven, and the adsorption is mainly concentrated on the surface, making it difficult to enter interlayer reactions.

4 Conclusion

In conclusion, we proposed novel coal gangue-based multiphase porous ceramic for high performance heavy metal cations removal adsorbent. Benefitting from the unique porous structure and chemical group, the coal gangue-based multiphase porous ceramic adsorbent exhibits outstanding performance of the removal of Cu^{2+}, Co^{2+}, and Ni^{2+} from wastewater. Furthermore, the microstructure and chemical composition have been revealed by several characterizations. Besides, the structure-function relationship between various reaction conditions and adsorption performance and the microstructure of adsorbent has been researched. Of note, the adsorption mechanism of complex porous ceramics on Cu^{2+}, Co^{2+}, and Ni^{2+} has been explored by simulated calculation. This coal gangue-based adsorbent and corresponding design strategy may shed light on development of effective and low-cost adsorbent for treatment of wastewater.

Data availability statement

The original contributions presented in the study are included in the article/Supplementary Material, further inquiries can be directed to the corresponding author.

Author contributions

XZ: Visualization, Conceptualization, Data curation, Formal Analysis, Investigation, Methodology, Software, Validation, Writing – original draft. YW: Visualization, Funding acquisition, Supervision, Writing – review and editing. RL: Writing – original draft, Data curation. RZ: Validation, Visualization, Supervision, Writing – review and editing. YM: Validation, Visualization, Writing – review and editing.

Funding

The author(s) declare that financial support was received for the research and/or publication of this article. This paper is financially supported by the National Natural Science Foundation of China (52371231) and Central Government Guides Local Science and Technology Development Special Fund Project (YDZJSX2022B003).

Acknowledgments

The work was carried out Shanxi Supercomputing Center of China, and the calculations were performed on TianHe-2. We also thank editors and reviewers for their efforts.

Conflict of interest

The authors declare that the research was conducted in the absence of any commercial or financial relationships that could be construed as a potential conflict of interest.

Publisher's note

Supplementary material

The Supplementary Material for this article can be found online at: https://www.frontiersin.org/articles/10.3389/fmats.2025.1414085/full#supplementary-material

References

Aksay, I. A., and Pask, J. A. (1974). The silica-alumina system: stable and metastable equilibria at 1.0 atmosphere. *Atmos. Sci.* 183 (4120), 69–71. doi:10.1126/science.183.4120.69

Chen, Y., Wang, N., Ola, O., Xia, Y., and Zhu, Y. (2021). Porous ceramics: light in weight but heavy in energy and environment technologies. *Mater. Sci. Eng. R Rep.* 143, 100589. doi:10.1016/j.mser.2020.100589

Dawodu, F. A., and Akpomie, K. G. (2014). Simultaneous adsorption of Ni (II) and Mn (II) ions from aqueous solution unto a Nigerian kaolinite clay. *J. Mater. Res. Technol.* 3 (2), 129–141. doi:10.1016/j.jmrt.2014.03.002

Deng, J., Liu, Y., Liu, S., Zeng, G., Tan, X., Huang, B., et al. (2017). Competitive adsorption of Pb (II), Cd (II) and Cu (II) onto chitosan-pyromellitic dianhydride modified biochar. *J. Colloid Interface Sci.* 506, 355–364. doi:10.1016/j.jcis.2017.07.069

Eren, E., and Afsin, B. (2008). An investigation of Cu (II) adsorption by raw and acid-activated bentonite: a combined potentiometric, thermodynamic, XRD, IR, DTA study. *J. Hazard. Mater.* 151 (2-3), 682–691. doi:10.1016/j.jhazmat.2007.06.040

Fonseca, B., Maio, H., Quintelas, C., Teixeira, A., and Tavares, T. (2009). Retention of Cr (VI) and Pb (II) on a loamy sand soil: kinetics, equilibria and breakthrough. *Chem. Eng. J.* 152 (1), 212–219. doi:10.1016/j.cej.2009.04.045

Gu, S., Kang, X., Wang, L., Lichtfouse, E., and Wang, C. (2019). Clay mineral adsorbents for heavy metal removal from wastewater: a review. *Environ. Chem. Lett.* 17, 629–654. doi:10.1007/s10311-018-0813-9

Guo, H., Li, W., and Ye, F. (2016). Preparation of microporous mullite ceramics by foaming for high temperature thermal isolation. *Ceram. Int.* 42 (15), 17332–17338. doi:10.1016/j.ceramint.2016.08.029

Guo, X., Jiang, W., Du, D., and Shang, X. (2023). Plackett-Burman experimental design of modified wood ceramics for ammonia nitrogen removal from water and response optimization of the modified wood ceramic's comprehensive performance. *Ceram. Int.* 49 (7), 11612–11622. doi:10.1016/j.ceramint.2022.12.008

Han, L., Li, F., Deng, X., Wang, J., Zhang, H., and Zhang, S. (2017). Foam-gelcasting preparation, microstructure and thermal insulation performance of porous diatomite ceramics with hierarchical pore structures. *J. Eur. Ceram. Soc.* 37 (7), 2717–2725. doi:10.1016/j.jeurceramsoc.2017.02.032

Jiao, Y., Zhu, J., Ge, J., Shi, C., Tai, Y., Huang, Y., et al. (2023). Design and fabrication of the ceramic composites via *in-situ* oxidized process: phase and microstructure evolution in *in-situ* oxidized SiC/Al-Mg-Si process. *Ceram. Int.* 49 (1), 1513–1520. doi:10.1016/j.ceramint.2022.10.202

Kim, G., Ku, S., Jung, Y., Park, Y. S., Choi, G. H., Hwang, S. S., et al. (2024). Ion-exchangeable and sorptive reinforced membranes for efficient electrochemical removal of heavy metal ions in wastewater. *J. Clean. Prod.* 438, 140779, doi:10.1016/j.jclepro.2024.140779

Li, X., Pan, M., Tao, M., Liu, W., Gao, Z., and Ma, C. (2022). Preparation of high closed porosity foamed ceramics from coal gangue waste for thermal insulation applications. *Ceram. Int.* 48 (24), 37055–37063. doi:10.1016/j.ceramint.2022.08.280

Li, Y., Li, G. Q., Li, Y., Deng, Y., and Deng, L. (2016). Development and application of an UHPLC-MS method for comparative pharmacokinetic study of phenolic components from dragon's blood in rats under simulated microgravity environment. *J. Pharm. Biomed. Anal.* 121, 91–98. doi:10.1016/j.jpba.2016.01.014

Luo, J., Hong, X., Qu, L., Luo, H., Ganiyu, S. O., Chelme-Ayala, P., et al. (2024). Decomplexation of copper complexes from synthetic and real electroplating wastewater by alkaline-thermal synergistic activation of persulfate and stabilization of generated sludge by Fe_3O_4 coating. *Chem. Eng. J.* 484, 149323, doi:10.1016/j.cej.2024.149323

Martra, G., Coluccia, S., Marchese, L., Augugliaro, V., Loddo, V., Palmisano, L., et al. (1999). The role of H2O in the photocatalytic oxidation of toluene in vapour phase on anatase TiO_2 catalyst: a FTIR study. *Catal. Today* 53 (4), 695–702. doi:10.1016/s0920-5861(99)00156-x

Mazarji, M., Bayero, M. T., Minkina, T., Sushkova, S., Mandzhieva, S., Bauer, T. V., et al. (2023). Nanomaterials in biochar: review of their effectiveness in remediating heavy metal-contaminated soils. *Sci. Total Environ.* 880, 163330. doi:10.1016/j.scitotenv.2023.163330

Mei, Y., Pang, J., Wang, X., Chen, E., Wu, D., and Ma, J. (2023). Coal gangue geopolymers as sustainable and cost-effective adsorbents for efficient removal of Cu (II). *Environ. Technol. Innov.* 32, 103416. doi:10.1016/j.eti.2023.103416

Musso, T. B., Parolo, M. E., Pettinari, G., and Francisca, F. (2014). Cu (II) and Zn (II) adsorption capacity of three different clay liner materials. *J. Environ. Manag.* 146, 50–58. doi:10.1016/j.jenvman.2014.07.026

Park, J. H., Ok, Y. S., Kim, S. H., Cho, J. S., Heo, J. S., Delaune, R. D., et al. (2016). Competitive adsorption of heavy metals onto sesame straw biochar in aqueous solutions. *Chemosphere* 142, 77–83. doi:10.1016/j.chemosphere.2015.05.093

Qasem, N. A., Mohammed, R. H., and Lawal, D. U. (2021). Removal of heavy metal ions from wastewater: a comprehensive and critical review. *npj Clean Water* 4 (1), 36. doi:10.1038/s41545-021-00127-0

Ren, J., Zheng, L., Su, Y., Meng, P., Zhou, Q., Zeng, H., et al. (2022). Competitive adsorption of Cd (II), Pb (II) and Cu (II) ions from acid mine drainage with zero-valent iron/phosphoric titanium dioxide: XPS qualitative analyses and DFT quantitative calculations. *Chem. Eng. J.* 445, 136778. doi:10.1016/j.cej.2022.136778

Roy, J., Chandra, S., Das, S., and Maitra, S. (2014). Oxidation behaviour of silicon carbide-a review. *Rev. Adv. Mater. Sci.* 38 (1), 29–39. doi:10.1007/s12633-019-00147-z

Sui, X., Pu, H., Maity, A., Chang, J., Jin, B., Lu, G., et al. (2020). Field-effect transistor based on percolation network of reduced graphene oxide for real-time ppb-level detection of lead ions in water. *ECS J. Solid State Sci. Technol.* 9 (11), 115012. doi:10.1149/2162-8777/abaaf4

Sun, J., Zhou, C., Shen, H., Du, J., Li, Q., Wu, W., et al. (2022). Green synthesis of ceramsite from industrial wastes and its application in selective adsorption: performance and mechanism. *Environ. Res.* 214, 113786. doi:10.1016/j.envres.2022.113786

Tan, B., Fu, A., Guo, L., Ran, Y., Xiong, J., Marzouki, R., et al. (2023). Insight into anti-corrosion mechanism of *Dalbergia odorifera* leaves extract as a biodegradable inhibitor for X70 steel in sulfuric acid medium. *Industrial Crops Prod.* 194, 116106. doi:10.1016/j.indcrop.2022.116106

Velarde, L., Nabavi, M. S., Escalera, E., Antti, M. L., and Akhtar, F. (2023). Adsorption of heavy metals on natural zeolites: a review. *Chemosphere* 328, 138508. doi:10.1016/j.chemosphere.2023.138508

Wei, C., Guo, W., Pratomo, E. S., Wang, D., Whitehead, D., et al. (2020). High speed, high power density laser-assisted machining of Al-SiC metal matrix composite with significant increase in productivity and surface quality. *J. Mater. Process. Technol.* 285, 116784. doi:10.1016/j.jmatprotec.2020.116784

Xia, F., Cui, S., and Pu, X. (2022). Performance study of foam ceramics prepared by direct foaming method using red mud and K-feldspar washed waste. *Ceram. Int.* 48 (4), 5197–5203. doi:10.1016/j.ceramint.2021.11.059

Xu, L., Liu, Y., Wang, J., Tang, Y., and Zhang, Z. (2021). Selective adsorption of Pb^{2+} and Cu^{2+} on amino-modified attapulgite: kinetic, thermal dynamic and DFT studies. *J. Hazard. Mater.* 404, 124140. doi:10.1016/j.jhazmat.2020.124140

Yan, S., He, P., Jia, D., Wang, Q., Liu, J., Yang, J., et al. (2018). Synthesis of novel low-cost porous gangue microsphere/geopolymer composites and their adsorption properties for dyes. *Int. J. Appl. Ceram. Technol.* 15 (6), 1602–1614. doi:10.1111/ijac.13045

Yao, G., Zhang, X., Sun, Z., and Zheng, S. (2019). High adsorption selectivity of zeolite X in the binary ionic system of Cu (II) and Zn (II). *J. Porous Mater.* 26, 1197–1207. doi:10.1007/s10934-019-00721-1

Zhang, Y., Wei, Z., Li, M., Wu, X., and Wang, W. (2020). Preparation and modification of mullite whiskers/cordierite porous ceramics for Cu^{2+} adsorption and removing. *ACS Omega* 5 (25), 15691–15701. doi:10.1021/acsomega.0c02085

Zhu, Q., Wu, J., Wang, L., Yang, G., and Zhang, X. (2016). Adsorption characteristics of Pb^{2+} onto wine lees-derived biochar. *Bull. Environ. Contam. Toxicol.* 97, 294–299. doi:10.1007/s00128-016-1760-4